Geophysical Research Letters

RESEARCH LETTER
10.1029/2022GL098776

# Seasonality of Continental Extratropical-Cyclone Wind Speeds Over Northeastern North America

**Ting-Chen Chen[1], Alejandro Di Luca, Katja Winger[1], René Laprise, and Julie M. Thériault**

[1]Centre Étude et simulation du climat à l'échelle régionale (ESCER)|Département des Sciences de la Terre et de l'atmosphère, Université du Québec à Montréal, Montréal, QC, Canada

**Key Points:**

- Extratropical-cyclone-associated 10-m wind speeds are the strongest in the fall season over northeastern North America
- Besides stronger continental cyclones and 850-hPa winds, weaker low-level stability in fall favors stronger 10-m wind speeds in this region
- Linear regression using 850-hPa wind, Richardson number, and surface roughness well predicts cyclones' 10-m wind speeds and seasonality

**Supporting Information:**

Supporting Information may be found in the online version of this article.

**Correspondence to:**

T.-C. Chen,
ting-chen.chen@courrier.uqam.ca

**Citation:**

Chen, T.-C., Di Luca, A., Winger, K., Laprise, R., & Thériault, J. M. (2022). Seasonality of continental extratropical-cyclone wind speeds over northeastern North America. *Geophysical Research Letters*, *49*, e2022GL098776. https://doi.org/10.1029/2022GL098776

Received 18 MAR 2022
Accepted 2 AUG 2022



**Abstract** This study investigates the seasonality of near-surface wind speeds associated with extratropical cyclones (ETCs) over northeastern North America using a global reanalysis data set during 1979–2020. As opposed to most studies that emphasize winter storms, ETCs during the fall exhibit significantly stronger 10-m winds over this region due to the slightly stronger continental cyclones and significantly weaker low-level stability during that time of the year. Also, ETCs favor inland lakes and Hudson Bay during the low-ice-content fall season, leading to lower surface roughness. Combining these results, we derive simple linear regressions to predict the 10-m wind speed given three variables: 850-hPa wind speed, low-level Richardson number, and surface roughness length. This formula captures the observed seasonality and serves as a valuable tool for cyclone near-surface wind risk assessment.

**Plain Language Summary** Extratropical cyclones can bring powerful winds that can cause severe damage to infrastructure. We find that cyclones with severe winds are the most frequent in the fall season over continental northeastern North America. Three reasons are found responsible: stronger continental cyclones, weaker low-level atmospheric stability, and the lower surface roughness over lakes and Hudson Bay, where cyclones frequently occur in fall. A simple formula that can effectively assess the near-surface wind speeds associated with cyclones is derived based on these results.

## 1. Introduction

One of the hazards associated with extratropical cyclones (ETCs) is the near-surface strong winds, causing damage to properties and infrastructure (Botzen et al., 2010; Hoeppe, 2016; Hudson et al., 2020). While extreme winds can be triggered by localized mesoscale processes (Golden & Snow, 1991), ETCs are a major contributor. Over the northeastern US, Booth et al. (2015) showed that 80% of the high-wind events, defined as at least five stations recording wind speeds exceeding the station-specific 1-year return levels, are associated with ETCs in winter. Over Europe, Owen et al. (2021) found that, on average, 81% of extreme wind events (above the grid-point 99th percentile) are associated with ETCs from October to March.

Most studies on windstorms focus on the winter season (Befort et al., 2019; Booth et al., 2015; Deroche et al., 2014; Martius et al., 2016; Schwierz et al., 2010), when the large-scale ETC activity reaches the annual maximum due to the peak of meridional temperature gradient (Hodges et al., 2011; Hoskins & Hodges, 2019; Shaw et al., 2016). However, ETC characteristics vary regionally and seasonally, and damaging windstorms may prevail in seasons other than winter. For Eastern Canada, a famous autumntime "Halloween Storm" caused insured losses of over CA$250 million in 2019 (Insurance Bureau of Canada, 2019). During its passage, multiple provinces recorded wind gusts exceeding 100 km $hr^{-1}$, leading to downed trees and power lines and one of the biggest power outages in the Quebec province (Government of Canada, 2020). Letson et al. (2021) extracted the top 10 most intense windstorms in the northeastern US during the last 4 decades based on the spatial extent of local extreme wind speeds at the 100-m height using the European Center for Medium-Range Weather Forecasts ERA5 reanalysis (Hersbach et al., 2020). In their list, 8 out of 10 were observed in fall (SON) and spring (MAM), while only 2 occurred in winter (DJF). While some studies examined the intra-annual variation of regional high-wind events (Murley et al., 2021), the link to the seasonality of ETCs remains understudied. This work, therefore, aims to characterize and explore the regional seasonal variation of near-surface wind speeds directly associated with ETCs.

Our study region targets continental northeastern North America (hereafter NNA; Figure 1a) for its high ETC frequency. This area includes the Great Lakes and Hudson Bay, which provide enhanced heat fluxes for ETCs

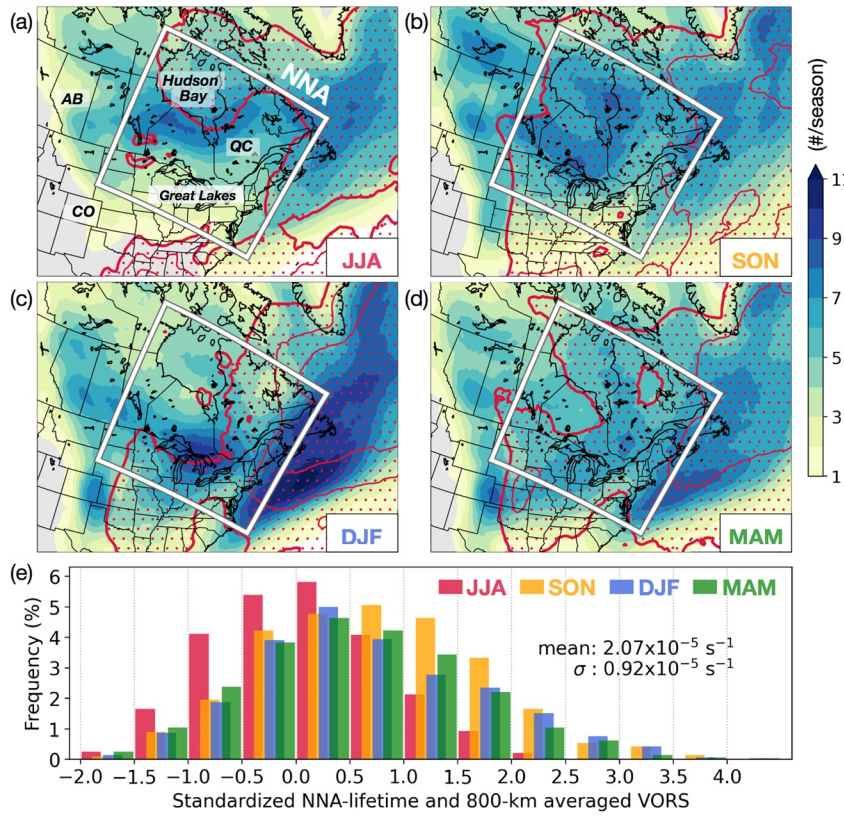


**Figure 1.** Average track density (shaded; number per season; each track is marked with a 250-km radius) and storm intensity (dotted regions for VORSmax $\geq 7 \times 10^{-5}$ s$^{-1}$ and every contour indicates an increment of $2 \times 10^{-5}$ s$^{-1}$) for (a) JJA, (b) SON, (c) DJF, and (d) MAM during 1979–2020. White square circumscribes the northeastern North America (NNA) region. (e) Frequency distribution (%) of standardized VORS (spatiotemporally averaged as described in Section 2.3) for NNA storms. Every bin interval is 0.5 standard deviation ($\sigma$). Key geographical regions in this study are indicated in (a) (QC for Quebec, AB for Alberta and CO for Colorado).

and is where two primary continental cyclone tracks merge in four seasons: Colorado Lows move northeastward, and Alberta Clippers track eastward (Reitan, 1974, Figure 12; Poan et al., 2018). Wind impact assessments often target the near-surface level for its pertinence to damages, and it is common to consider either the instantaneous wind field (Befort et al., 2019; Booth et al., 2015; Deroche et al., 2014) or the wind gust (Martius et al., 2016; Owen et al., 2021; Schwierz et al., 2010). We assess both variables at the 10-m height from the ERA5 reanalysis database, and the presenting results focus on the instantaneous wind while the wind gust is discussed in Section 4. As the near-surface wind can be affected by the synoptic-scale ETC circulation and the boundary-layer and surface properties, we also examine the wind speed at 850-hPa, low-level stability, and surface roughness. The goal is to investigate whether there is a statistically significant seasonal variation of ETC 10-m wind speed and how it relates to other variables. Finally, we use linear regression models to further quantify such associations and to seek a tool for ETC near-surface wind prediction.

The paper is structured as follows: Section 2 details the data and methodology. Section 3 reports the seasonality of ETC wind speeds and the connection to other properties over NNA. Based on these results, linear regression models for ETC near-surface wind speed prediction are built. Section 4 discusses the sensitivity and validity of our results, and Section 5 presents the conclusion.

## 2. Data and Methodology

In this study, all analyses are conducted using the ERA5 hourly reanalysis at a spatial resolution of $0.25 \times 0.25$ from January 1979 to December 2020. The validity of ERA5 10-m wind speed for ETCs has been examined using in situ station observations, where available, from the NOAA Integrated Surface Database (ISD; Smith

et al., 2011) for 10 years from 2010 to 2019. Overall, ERA5 agrees well with ISD in the spatially averaged values for ETCs. The averaged wind speeds over all ISD stations and their closest ERA5 grid points within an 800-km radius of ETCs show similar ranges from 1 to 11 m/s (Figure S1 in Supporting Information S1). The root-mean-square error (RMSE) of 0.68 m/s is small, and the *R*-squared value indicates that ERA5 can capture 84% of the variability in ISD. More importantly, the seasonal variations between ERA5 and ISD exhibit strong agreement despite the overall larger medians of ERA5 (Figure S2 in Supporting Information S1). More details can be found in the Supporting Information S1.

### 2.1. Storm Tracking Algorithm

To identify cyclone tracks, a storm tracking algorithm modified from Chartrand and Pausata (2020) is performed in a region covering North America and part of the Pacific and Atlantic Oceans (20–80°N, 180–0°W). The main steps are described below:

1. We first apply a Cressman filter with a 400-km influence radius to spatially smooth the 850-hPa relative vorticity (VORS) and the mean sea-level pressure fields.
2. ETC centers are identified based on two conditions: the center must be a local minimum in the mean sea-level pressure, and the maximum VORS (VORSmax) within a 400-km diameter must be larger than $10^{-5}$ $s^{-1}$. This threshold has been used in other studies (Priestley et al., 2020). Only the lowest pressure center is retained if two or more low-pressure centers are found in this circular region.
3. For every existing storm at the current time ($t_0$), the algorithm first predicts its next location by assuming that the storm shifts in the same direction and distance as its two previous locations (when available). Then, the matching is performed by finding the closest storm center at $t_1$ whose distance to the predicted location is smaller than the shifting distance or a specified threshold, whichever is greater. We choose 100 km for this threshold, considering that the translation speed of ETCs is about 50 km/hr on average (Bernhardt & DeGaetano, 2012). The threshold is extended to 150 km if the pressure of the center to be matched deviates less than ± 3 hPa from the existing storm's value at $t_0$.
   If no matching is found, the program changes the prediction with zero shift and repeats the matching. If it still finds no match, the tracking of the existing storm ends. The centers that cannot be matched will be viewed as new tracks.
4. Cyclone tracks lasting less than 24 hr or traveling a distance smaller than 1,000 km are discarded to filter out thermal lows and other small systems.

Our tracking results qualitatively agree with past studies, with high cyclone center density over the maritime storm tracks and on the lee-sides of the Rockies, Great Lakes, and the Hudson Bay over North America (Neu et al., 2013; Figure S3 in Supporting Information S1). While the magnitude of cyclone center density varies significantly across different algorithms, our result lies within the reported range but in the lower part of 15 commonly-used ETC tracking algorithms presented in Neu et al. (2013).

### 2.2. Sub-Selection of Inland Storms

To target ETCs that had distinct impacts over the region of interest, we select storms whose centers had been within NNA for at least 24 hr for further analyses. This sub-selection contains 2,766 ETCs, about 11.2% of all tracked storms during 1979–2020.

### 2.3. Calculation for Storm Characteristics

ETC-associated characteristics are calculated by averaging over a circular region around the center and then over the duration when the center was within the NNA region. The variables include the wind speeds at 10-m height (10WS) and 850-hPa level (850WS), the bulk Richardson number ($Ri_b$), and the surface roughness length ($z_0$). For the spatial average, a fixed radius of 800 km is used. Although this moderate radius may not always cover the entire frontal winds, ETC composite analysis usually shows the strongest wind speeds within a radius of 1,000 km (Field & Wood, 2007). The sensitivity to different radii is discussed in Section 4.

In this study, variables are sometimes expressed in standardized values to highlight the deviation from the climatology of all ETCs in NNA. For example, a zero standardized 10WS implies that the storm has an averaged 10WS,

while a larger-than-one value indicates that the 10WS is stronger than the mean by more than one standard deviation. We consider the latter cases as severe events.

### 2.4. Statistical Significance Testing

To determine the statistical significance of differences among seasons, we conduct the two-sample Kolmogorov-Smirnov test with the null hypothesis that both samples (i.e., any two seasons) come from the same population. Distributions of two seasons are considered significantly different if the null hypothesis is rejected at the significance level of 0.01. The Pearson correlation coefficients presented hereafter are all significant at the 0.01 level based on the Student's *T*-test.

## 3. Results

### 3.1. Seasonality of Cyclone Tracks and Intensity

Track density represents the number of ETC tracks passing a grid cell, and repetitive entries of the same storm at the same location are counted only once (Neu et al., 2013). The highest track density is found in DJF over the North Atlantic Gulf Stream, that is, the midlatitude maritime storm tracks. Over inland, all seasons exhibit comparable magnitudes with some spatial variations (Figures 1a–1d). While the Great Lakes region still shows a maximum in DJF, Hudson Bay exhibits a higher track density in SON.

Two storm intensity measures are examined: VORSmax and the 800-km-averaged VORS, both averaged over the ETC lifetime in NNA. VORSmax peaks in DJF ($>1 \times 10^{-4}$ s$^{-1}$) downstream to the track density maximum (Figures 1a–1d). For inland, VORSmax $>7 \times 10^{-5}$ s$^{-1}$ only cover part of the NNA region in DJF, while they extend to almost the entire domain in SON and MAM. While the frequency distribution of VORSmax shows a clear predominance of severe ETCs in SON, closely followed by MAM (not shown), the 800-km-averaged VORS exhibits comparable cases of very severe ETCs (>2 standardized VORS) among SON, MAM, and DJF (Figure 1e). Note that for NNA region, JJA, SON, DJF, and MAM constitute 24.6%, 27.8%, 23.7%, and 23.9% of total cases, respectively.

### 3.2. Seasonality of Wind Speeds

Figure 2 shows the wind speed distribution of NNA ETCs in different seasons in standardized 850WS and 10WS. Qualitatively consistent with the storm intensity, the seasonal distribution of 850WS (Figure 2a) shows the highest median in SON (standardized value of 0.2), followed by MAM (0.07), DJF (−0.02), and JJA (−0.6) (Figure 2a). Such differences among seasons are not statistically significant except when compared with JJA (Figure 2a). In contrast, the seasonal distributions of 10WS are significantly different from each other (Figure 2b). The median of 10WS is positive only for SON storms with a standardized value of 0.2, compared with −0.006, −0.3, and −0.5 for MAM, DJF, and JJA storms, respectively (Figure 2b). Note that in situ observations, despite their heterogeneous distribution over NNA, also show the highest median of ETC 10WS in SON (Figure S2 in Supporting Information S1). Overall, stronger 10WS are correlated with stronger 850WS with a Pearson correlation coefficient of 0.81 (Figure 2c). Interestingly, severe 10WS cases (standardized wind speeds >1) are predominant in SON, regardless of the associated 850WS being severe or not. Combining the upper quadrants in Figure 2c indicates that 26%, 16%, and 15% of the SON, MAM, and DJF storms exhibit severe 10WS, respectively. Note that ETCs with severe 850WS but non-severe 10WS (the lower-right quadrant) are the most frequent in DJF.

From another perspective, among all ETCs with severe 10WS over NNA during 1979–2020, 44% (196 out of 447 cases) occurred in SON, 24% in MAM, 21% in DJF, and 11% in JJA. Consistent results are shown in terms of wind speed ratio, 10WS/850WS (Figure 2d). Excluding JJA for its significantly lowest 850WS, the highest wind speed ratio in SON indicates a greater 10WS given the same driving 850WS compared to MAM and DJF ETCs.

### 3.3. Seasonality of Near-Surface Stability and Surface Roughness

Many studies showed that a less stable boundary layer favors stronger near-surface winds as greater turbulent mixing aids downward momentum transport (O'Neill, 2012; Jakobson et al., 2019). Sampe and Xie (2007) indicated a strong correlation between boundary-layer instability and high-wind occurrence over oceans from satellite

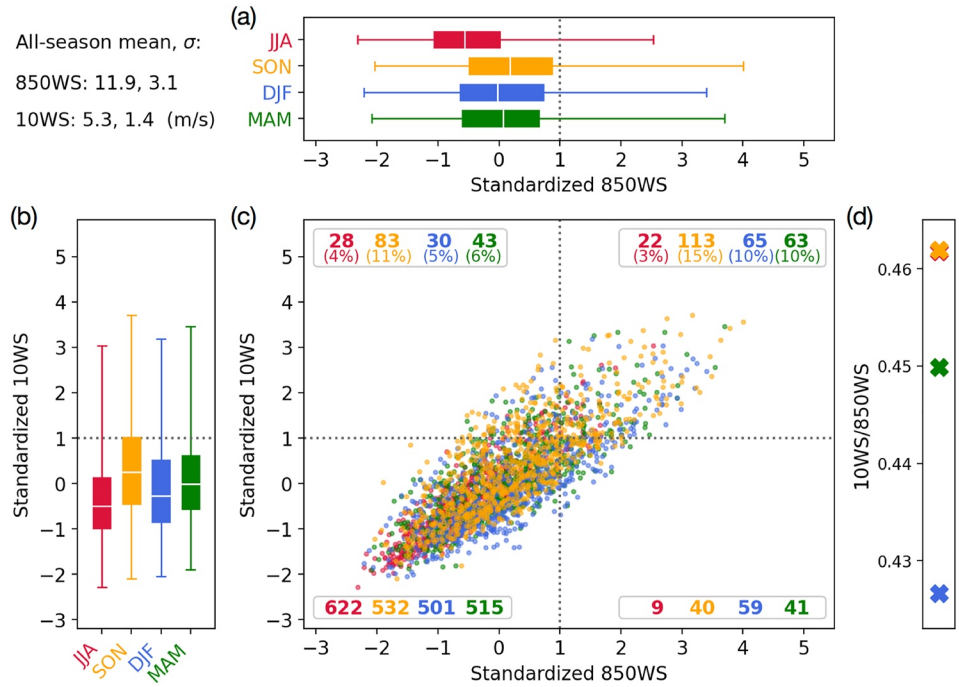


**Figure 2.** Boxplots of standardized (a) 850WS and (b) 10WS for storms in four seasons. The whiskers here refer to the minima and maxima. (c) Scatter plot of storms in the coordinate of 850WS ($x$-axis)-10WS ($y$-axis). Colors red for JJA, orange for SON, blue for DJF, and green for SON. The mean and standard deviation for the standardization are indicated in the upper-left corner. Four quadrants are separated by one standardized 850WS and 10WS to differentiate the non-severe and severe events (gray dotted lines). The case numbers are indicated in bold. The percentages in parentheses are calculated with respect to each seasonal sum. (d) The averaged value of wind speed ratio for storms in each season (JJA is overlapped by SON).

observations. Booth et al. (2010) found distinct spatial patterns of maritime storm tracks at 850-hPa and at 10 m, as the latter is enhanced in regions of strong instability. Here, we calculate the bulk Richardson number ($Ri_b$; Zoumakis & Kelessis, 1991) for the air layer between the two lowest ERA5 model levels (about 9 and 38 m height over NNA):

$$Ri_b = \frac{\text{buoyancy term}}{\text{shear term}}, \text{ where}$$

$$\text{buoyancy term} = \frac{g}{\theta_v^{\text{low}}} \frac{\theta_v^{\text{upp}} - \theta_v^{\text{low}}}{z^{\text{upp}} - z^{\text{low}}}, \text{and shear term} = \left( \frac{V^{\text{upp}} - V^{\text{low}}}{z^{\text{upp}} - z^{\text{low}}} \right)^2, \quad (1)$$

with $g$ for the gravity, $\theta_v$ the virtual potential temperature, $z$ the height, and $V$ the horizontal wind speed. Superscripts upp and low indicate upper and lower levels, respectively. A lower $Ri_b$ indicates a weaker stability.

Overall, a negative correlation is found between 10WS and $Ri_b$ with a Pearson correlation coefficient of −0.47. Furthermore, the seasonal variation of $Ri_b$ is qualitatively reversed to that of 10WS, indicating the importance of $Ri_b$ in affecting the seasonality of ETC 10-m wind speeds (Figures 2b and 3a). The lowest median of 0.05 occurs in SON and the highest value of 0.21 appears in JJA, with intermediate values of 0.14 in both DJF and MAM. To better understand the seasonality, ETC-associated $Ri_b$ is separated into subcomponents over land and over water/ice (Figures 3a, 3b, and 3e). On average, about 80% of the 800-km impact region of the storm is over the land surface, with a slightly higher land cover for DJF storms and a higher water/ice cover for JJA storms (stars in Figure 3a). The seasonal variation of $Ri_b$ over water is much larger than that over land, and so the former substantially affects the overall seasonality despite the smaller water cover fraction. For example, the high $Ri_b$ over water overpowers the low $Ri_b$ over land in JJA storms, and the low $Ri_b$ over water counteracts the high $Ri_b$ over land in DJF storms. For SON, $Ri_b$ over water and land are both relatively low, favoring strong 10-m winds.

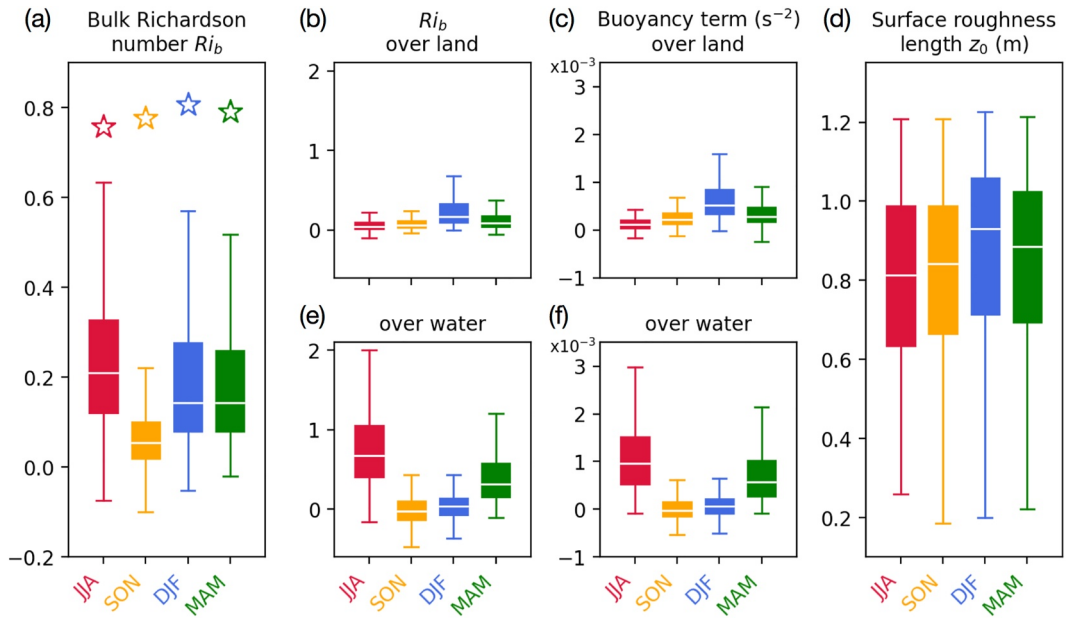


**Figure 3.** Boxplot showing the distribution of extratropical cyclone (ETC)-associated (a) $Ri_b$, and its sub-component averaged (b) over land and (e) over water/ice in four seasons. The stars in (a) indicate the median values of the land cover fraction in the 800-km-radius ETC region in different seasons. (c) and (f) Same as (b) and (e), respectively, but for the numerator of $Ri_b$ in Equation 1, that is, the buoyancy term ($s^{-2}$). (d) Same as (a) but for $z_0$ (m).

The contrasting seasonal cycles of $Ri_b$ over land and water are dominated by changes in the buoyancy term, mainly due to the different heat capacities over water, ice and land (Figures 3c and 3f). Taking JJA as an example, while the air temperature near the land surface warms up quickly, the air near the water surface remains relatively cool, hence resulting in weakly stratified thermal structures above land but strongly stratified structures above water/ice. Another factor that may contribute to the buoyancy over water is the ice cover. Examining the ERA5 daily updated sea-ice cover, that is, the fraction of a water-body grid box covered by ice, shows that the NNA-averaged value peaks at 0.7 in February/March, drops to nearly 0 in July/August, and remains below 0.1 during SON (not shown). The low ice cover in SON indicates more open-water areas with substantial heat fluxes and weak stratifications above (Vihma, 2014).

Another critical factor for 10WS is the aerodynamic roughness length ($z_0$). A larger $z_0$ indicates a higher surface resistance, slowing the near-surface winds. Our analysis shows a negative Pearson correlation coefficient between 10WS and $z_0$ of −0.41. Consistent with the seasonality of land cover fraction, the median of $z_0$ is the largest for DJF (0.93 m) and smallest for JJA (0.81 m). However, the difference among seasons is not always statistically significant, except when compared with the large $z_0$ in DJF. Note that in SON, the lower ice content also implies a lower $z_0$ (Jakobson et al., 2019), but such water-ice difference has a small impact as $z_0$ over land is a few orders of magnitude larger than that over water/ice.

### 3.4. Linear Regression Models for 10-m Wind Speed

To quantify the relative importance of 850WS, $Ri_b$, $z_0$ in 10-m wind speeds, we apply ordinary least squares linear regression models using the Scikit-learn machine learning library for Python (Pedregosa et al., 2011). First, we consider a benchmark model with only one predictor variable 850WS to predict 10WS for each ETC, and the best fit result gives a formula:

$$10\mathrm{WS}^p = a_1 \cdot 850\mathrm{WS} + 1.09, \quad (2)$$

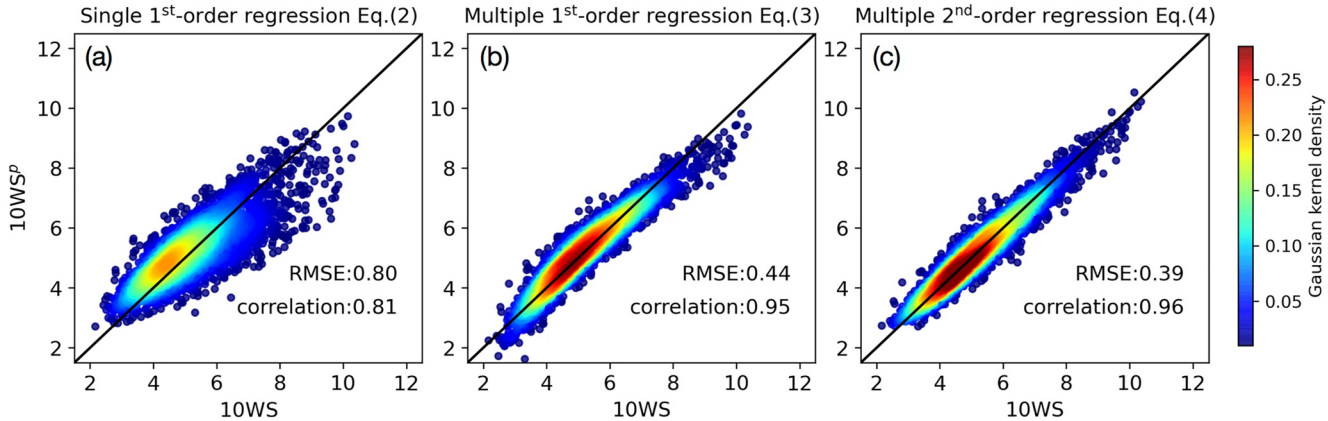


**Figure 4.** Scatter plot of 10WS ($x$-axis) and 10WS$^p$ ($y$-axis) for all extratropical cyclones in northeastern North America. The prediction is derived from the (a) single linear regression in Equation 2, (b) multiple linear regression in Equation 3, and (c) multiple linear regression in Equation 4. The black diagonal lines indicate the perfect prediction. Colors indicate the Gaussian kernel density of the data.

where the regression coefficient $a_1 = 0.35$, and superscript $p$ indicates the predicted value. The Pearson correlation coefficient between the predicted and observed 10WS is 0.81 and the RMSE is 0.8 m s$^{-1}$ (Figure 4a). In contrast, the linear regression model with the inclusion of $Ri_b$ and $z_0$ gives:

$$10\text{WS}^p = a_1 \cdot 850\text{WS} - a_2 \cdot Ri_b - a_3 \cdot z_0 + 3.97, \quad (3)$$

with regression coefficients of $a_1 = 0.33$, $a_2 = 1.28$ m s$^{-1}$, and $a_3 = 2.90$ s$^{-1}$. Equation 3 notably improves the 10WS$^p$, with the correlation coefficient increasing to 0.95 and the RMSE dropping by 45% to 0.44 m s$^{-1}$ (Figure 4b).

Further improvements with RMSE reduced to 0.39 m s$^{-1}$ can be achieved by including the higher-order interaction terms (Figure 4c):

$$10\text{WS}^p = a_1 \cdot 850\text{WS} + a_2 \cdot Ri_b - a_3 \cdot z_0 - a_4 \cdot 850\text{WS} \cdot Ri_b - a_5 \cdot 850\text{WS} \cdot z_0 + 1.25, \quad (4)$$

where $a_1$ to $a_5$ are 0.58, 1.61 m s$^{-1}$, 0.06 s$^{-1}$, 0.30, and 0.25 m$^{-1}$, respectively. Equation 4 indicates that the free-tropospheric winds modulate the net effects of stability and surface roughness. For example, given $z_0 = 0.4$ m and 850WS = 10 m s$^{-1}$, a decrease in $Ri_b$ from 0.6 to −0.2 leads to a 21% increase of 10WS$^p$ (from 5.2 to 6.3 m s$^{-1}$). In contrast, with 850WS = 30 m s$^{-1}$, the same decrease of $Ri_b$ results in a 53% increase of 10WS$^p$ (from 11.2 to 17.1 m s$^{-1}$).

The simplicity of Equation 3 allows us to further estimate the contribution of each factor to the seasonality of near-surface winds (Figure S4 in Supporting Information S1). The 10WS$^p$ seasonal mean is 5.7, 5.3, 5.3, and 4.7 m s$^{-1}$ in SON, MAM, DJF, and JJA, respectively, all of which deviate no more than 2% from their observed 10WS. By defining seasonality as the difference of any two seasonal means, we can calculate how much the difference of each right-hand-side term accounts for the net difference of 10WS$^p$. Our results show that compared to JJA, the higher 10WS$^p$ in SON is explained by the higher 850WS (78%) and lower $Ri_b$ (22%). For the seasonality between DJF and SON, 29%, 39%, and 32% of the higher 10WS$^p$ in SON is related to the higher 850WS, lower $Ri_b$ and lower $z_0$, respectively. Between MAM and SON, the contribution from the higher 850WS, lower $Ri_b$, and lower $z_0$ to the higher 10WS$^p$ in SON is about 41%, 35%, and 24%, respectively. In all, both 850WS and $Ri_b$ have comparable importance in affecting the seasonality of 10WS, especially the high values in SON.

## 4. Discussion

In complement to the 10WS analysis, we also examine the 10-m wind gust since previous post-processing (10WG) from ERA5. While the wind gust variable is more representative of storm impacts, it is sensitive to the gust parameterization in the operated model (Schwierz et al., 2010). Results show that despite an overall increase of magnitudes (9.5 and 5.3 m/s for all-case averages of 10WG and 10WS, respectively), the seasonal variation of 10WG agrees well with that of the 10WS after standardization (Figure S5 in Supporting Information S1).

Notably, compared to 10WS, 10WG exhibits a higher correlation with 850WS (Pearson correlation coefficient of 0.91 vs. 0.81). As 10WG is the sum of 10WS and the parameterized turbulent and convective gustiness (Minola et al., 2020), this result agrees with the importance of boundary-layer stability to near-surface winds. Because such an effect has been parameterized, the improvement for 10WG prediction from single to multiple linear regression is less evident than for 10WS (Figure S6 in Supporting Information S1).

The sensitivity to different radii ($R$) for calculating the ETC characteristics is also investigated. We utilize $R$ of 400, 600, and 1,000 km for the spatial averaging. The results remain qualitatively consistent and the predominance of severe 10WS in SON holds for all radii. However, the wind speed ratio decreases with $R$ for DJF storms while it increases for other-season storms, leading to a more robust seasonality at a larger $R$ (Figure S7 in Supporting Information S1). This reflects that DJF ETCs generally have larger sizes; thus, their spatially averaged 850WS maintains relatively high compared to storms in other seasons at larger $R$.

Finally, we emphasize that while in situ observational data may provide a more accurate description of the local reality than reanalysis, the latter has the advantage of spatiotemporally homogeneous coverage and can provide a more complete account of ETCs. Our preliminary comparison between ERA5 and ISD station data shows that, if only the ISD data is utilized, the calculated ETC wind speed is biased toward where observational stations are densely populated (see more in the Supporting Information S1). Nevertheless, when the comparison between ERA5 and ISD is made only when and where observational stations are available, they exhibit high agreement in capturing the ETC-associated 10WS and the seasonality.

## 5. Conclusions

This study investigates the seasonal variation of 10-m wind speeds (10WS) associated with continental ETCs, targeting the NNA region with the ERA5 reanalysis data during 1979–2020.

Whereas many studies on ETC high-wind events focused only on the winter season, we find that ETCs exhibiting severe 10WS occurred most frequently in SON (44%), compared to DJF (24%), MAM (21%), and JJA (11%). Such seasonality may be unique to the NNA region, where continental cyclones exhibit slightly stronger 850WS in SON and MAM, as opposed to the coastal region where intense oceanic ETCs often peak in DJF (Colle et al., 2015; Hirsch et al., 2001). More importantly, the stronger 10WS of SON storms is significantly attributed to the weaker low-level stability (the bulk Richardson number, $Ri_b$), favoring downward momentum transport from the free atmosphere. The NNA region contains sizable inland water bodies and is located on the periphery of the Arctic, both of which reinforce the seasonal variation of low-level stability. In addition, SON storms occur more frequently over inland water surfaces and thus experience lower surface roughness ($z_0$) than those over land surfaces in DJF and MAM.

Based on these results, a simple yet effective linear regression is derived to capture ETC-associated 10WS given 850WS, $Ri_b$, and $z_0$. This model outperforms the single linear regression considering only 850WS, with the RMSE in 10WS prediction decreased by 45%. In all, we highlight that the low-level stratification (turbulent mixing) and surface roughness should not be neglected for ETC wind-damage risk assessment and trend evaluation in climate studies.

## Data Availability Statement

The ERA5 reanalysis is available through the Climate Data Store infrastructure: https://cds.climate.copernicus.eu/cdsapp#!/dataset/reanalysis-era5-single-levels?tab=overview. Our extratropical cyclone track data and analysis is publicly available at https://doi.org/10.5683/SP3/LH8OBV (Chen et al., 2022).

**Acknowledgments**
This research has been conducted as part of the project "Simulation et analyse du climat à haute resolution" funded by the Electrification and Climate Change Fund, Government of Québec. We appreciate two anonymous reviewers' suggestions to improve this work. We also thank Francois Collet for helping evaluate ERA5 wind speed with the NOAA Integrated Surface Database.

## References

Befort, D. J., Wild, S., Knight, J. R., Lockwood, J. F., Thornton, H. E., Hermanson, L., et al. (2019). Seasonal forecast skill for extratropical cyclones and windstorms. *Quarterly Journal of the Royal Meteorological Society*, *145*(718), 92–104. https://doi.org/10.1002/qj.3406348

Bernhardt, J. E., & DeGaetano, A. T. (2012). Meteorological factors affecting the speed of movement and related impacts of extratropical cyclones along the U.S. East Coast. *Natural Hazards*, *61*(3), 1463–1472. https://doi.org/10.1007/s11069-011-0078-0

Booth, J. F., Rieder, H. E., Lee, D. E., & Kushnir, Y. (2015). The paths of extratropical cyclones associated with wintertime high-wind events in the Northeastern United States. *Journal of Applied Meteorology and Climatology*, *54*(9), 1871–1885. https://doi.org/10.1175/jamc-d-14-0320.1

Booth, J. F., Thompson, L. A., Patoux, J., Kelly, K. A., & Dickinson, S. (2010). The signature of the midlatitude tropospheric storm tracks in the surface winds. *Journal of Climate*, *23*(5), 1160–1174. https://doi.org/10.1175/2009jcli3064.1

Botzen, W., van den Bergh, J., & Bouwer, L. (2010). Climate change and increased risk for the insurance sector: A global perspective and an assessment for The Netherlands. *Natural Hazards*, *52*(3), 577–598. https://doi.org/10.1007/s11069-009-9404-1352

Chartrand, J. & Pausata, F. S. R. (2020). Impacts of the North Atlantic Oscillation on winter precipitations and storm track variability in southeast Canada and the northeast United States, *Weather and Climate Dynamics*, *1*, 731–744. https://doi.org/10.5194/wcd-1-731-2020

Chen, T.-C., Di Luca, A., & Winger, K. (2022). *North America extratropical cyclone (NAEC) catalogue*. Borealis. https://doi.org/10.5683/SP3/LH8OBV

Colle, B. A., Booth, J., & Chang, E. (2015). A review of historical and future changes of extratropical cyclones and associated impacts along the US eastcoast. *Current Climate Change Reports*, *1*(3), 125–143. https://doi.org/10.1007/s40641-015-0013-7

Deroche, M.-S., Choux, M., Codron, F., & Yiou, P. (2014). Three variables are better than one: Detection of European winter windstorms causing important damages. *Natural Hazards and Earth System Sciences*, *14*(4), 981–993. https://doi.org/10.5194/nhess-14-981-2014

Field, P. R., & Wood, R. (2007). Precipitation and cloud structure in midlatitude cyclones. *Journal of Climate*, *20*(2), 233–254. https://doi.org/10.1175/jcli3998.1

Golden, J. H., & Snow, J. T. (1991). Mitigation against extreme windstorms. *Reviews of Geophysics*, *29*(4), 477–504. https://doi.org/10.1029/91RG01814

Government of Canada. (2020). Canada's top 10 weather stories of 2019. Retrieved from https://www.canada.ca/en/environment%2Dclimate%2Dchange/services/top%2Dten%2Dweather%2Dstories/2019.html%23toc8

Hersbach, H., Bell, B., Berrisford, P., Hirahara, S., Horányi, A., Muñoz-Sabater, J., et al. (2020). The ERA5 global reanalysis. *Quarterly Journal of the Royal Meteorological Society*, *146*(730), 1999–2049. https://doi.org/10.1002/qj.3803

Hirsch, M. E., DeGaetano, A. T., & Colucci, S. J. (2001). An East Coast winter storm climatology. *Journal of Climate*, *14*(5), 882–899. https://doi.org/10.1175/1520-0442(2001)014<0882:AECWSC>2.0.CO;2

Hodges, K. I., Lee, R. W., & Bengtsson, L. (2011). A comparison of extratropical cyclones in recent reanalyses ERA-Interim, NASA MERRA, NCEP CFSR, and JRA-25. *Journal of Climate*, *24*(18), 4888–4906. https://doi.org/10.1175/2011jcli4097.1

Hoeppe, P. (2016). Trends in weather related disasters – Consequences for insurers and society. *Weather and Climate Extremes*, *11*, 70–79. https://doi.org/10.1016/j.wace.2015.10.002

Hoskins, B. J., & Hodges, K. I. (2019). The annual cycle of northern hemisphere storm tracks. Part I: Seasons. *Journal of Climate*, *32*(6), 1743–1760. https://doi.org/10.1175/JCLI-D-17-0870.1

Hudson, P., Ruig, L. D., de Ruiter, M., Kuik, O., Botzen, W., Den, X. L., et al. (2020). An assessment of best practices of extreme weather insurance and directions for a more resilient society. *Environmental Hazards*, *19*(3), 301–321. https://doi.org/10.1080/17477891.2019.1608148

Insurance Bureau of Canada. (2019). Halloween storm across Eastern Canada caused over $250 million in insured damage. Retrieved from http://www.ibc.ca/nl/resources/media-centre/media-releases/halloween-storm-across-eastern-canada-caused-over-250-million-in-insured-damage

Jakobson, L., Vihma, T., & Jakobson, E. (2019). Relationships between sea ice concentration and wind speed over the Arctic Ocean during 1979–2015. *Journal of Climate*, *32*(22), 7783–7796. https://doi.org/10.1175/JCLI-D-19-0271.1

Letson, F. W., Barthelmie, R. J., Hodges, K. I., & Pryor, S. C. (2021). Intense windstorms in the northeastern United States. *Natural Hazards and Earth System Sciences*, *21*(7), 2001–2020. https://doi.org/10.5194/nhess-21-2001-2021

Martius, O., Pfahl, S., & Chevalier, C. (2016). A global quantification of compound precipitation and wind extremes. *Geophysical Research Letters*, *43*(14), 7709–7717. https://doi.org/10.1002/2016GL070017

Minola, L., Zhang, F., Azorin-Molina, C., Safaei Pirooz, A. A., Flay, R. G. J., Herbach, H., & Chen, D. (2020). Near-surface mean and gust wind speeds in ERA5 across Sweden: Towards an improved gust parametrization. *Climate Dynamics*, *55*(3–4), 887–907. https://doi.org/10.1007/s00382-020-05302-6

Murley, V. A., Durkee, J. D., Gilliland, J. M., & Black, A. W. (2021). A climatology of convective and non-convective high-wind events across the eastern United States during 1973–2015. *International Journal of Climatology*, *41*(S1), E368–E379. https://doi.org/10.1002/joc.6690

Neu, U., Akperov, M. G., Bellenbaum, N., Benestad, R., Blender, R., Caballero, R., et al. (2013). IMILAST: A community effort to intercompare extratropical cyclone detection and tracking algorithms. *Bulletin of the American Meteorological Society*, *94*(4), 529–547. https://doi.org/10.1175/BAMS-D-11-00154.1

O'Neill, L. W. (2012). Wind speed and stability effects on coupling between surface wind stress and sst observed from buoys and satellite. *Journal of Climate*, *25*(5), 1544–1569. https://doi.org/10.1175/JCLI-D-11-00121.1

Owen, L. E., Catto, J. L., Stephenson, D. B., & Dunstone, N. J. (2021). Compound precipitation and wind extremes over Europe and their relationship to extratropical cyclones. *Weather and Climate Extremes*, *33*, 100342. https://doi.org/10.1016/j.wace.2021.100342

Pedregosa, F., Varoquaux, G., Gramfort, A., Michel, V., Thirion, B., Grisel, O., & Duchesnay, E. (2011). *Journal of Machine Learning Research*, *12*, 2825–2830.

Poan, E., Gachon, P., Laprise, R., Aider, R., & Dueymes, G. (2018). Investigating added value of regional climate modeling in North American winter storm track simulations. *Climate Dynamics*, *50*(5–6), 1799–1818. https://doi.org/10.1007/s00382-017-3723-9

Priestley, M. D. K., Ackerley, D., Catto, J. L., Hodges, K. I., McDonald, R. E., & Lee, R. W. (2020). An overview of the extratropical storm tracks in CMIP6 historical simulations. *Journal of Climate*, *33*(15), 6315–6343. https://doi.org/10.1175/jcli-d-19-0928.1

Reitan, C. H. (1974). Frequencies of cyclones and cyclogenesis for North America, 1951–1970. *Monthly Weather Review*, *102*(12), 861–868. https://doi.org/10.1175/1520-0493(1974)102<0861:FOCACF>2.0.CO;2

Sampe, T., & Xie, S. (2007). Mapping high wea winds from space: A global climatology. *Bulletin of the American Meteorological Society*, *88*(12), 1965–1978. https://doi.org/10.1175/bams-88-12-1965

Schwierz, C., Köllner-Heck, P., Mutter, E. Z., Bresch, D. N., Vidale, P.-L., Wild, M., & Schär, C. (2010). Modelling European winter wind storm losses in current and future climate. *Climatic Change*, *101*(3–4), 485–514. https://doi.org/10.1007/s10584-009-9712-1

Shaw, T. A., Baldwin, M., Barnes, E. A., Caballero, R., Garfinkel, C. I., Hwang, Y. T., et al. (2016). Storm track processes and the opposing influences of climate change. *Nature Geoscience*, *9*, 656–664. https://doi.org/10.1038/ngeo2783

Smith, A., Lott, N., & Vose, R. (2011). The integrated surface database: Recent developments and partnerships. *Bulletin of the American Meteorological Society*, *92*(6), 704–708. https://doi.org/10.1175/2011BAMS3015.1

Vihma, T. (2014). Effects of arctic sea ice decline on weather and climate: A review. *Surveys in Geophysics*, *35*(5), 1175–1214. https://doi.org/10.1007/s10712-014-9284-0

Zoumakis, N., & Kelessis, A. (1991). The dependence of the bulk richardson number on stability in the surface layer. *Boundary-Layer Meteorology*, *57*(4), 407–414. https://doi.org/10.1007/BF00120057